Controlled growth of a molecular bulk heterojunction photovoltaic cell

FAN YANG[1], MAX SHTEIN[2] AND STEPHEN R. FORREST[1]*

[1]Department of Electrical Engineering, [2]Department of Chemical Engineering, Princeton Institute for the Science and Technology of Materials (PRISM),Princeton University, Princeton, New Jersey 08544, USA

*e-mail: forrest@princeton.edu

Published online: 12 December 2004; doi:10.1038/nmat1285

The power conversion efficiency of organic photovoltaic cells has increased with the introduction of the donor–acceptor heterojunction that serves to dissociate strongly bound photogenerated excitons[1]. Further efficiency increases have been achieved in both polymer[2,3] and small-molecular-mass[4] organic photovoltaic cells through the use of the bulk heterojunction (BHJ), where the distance an exciton must diffuse from its generation to its dissociation site is reduced in an interpenetrating network of the donor and acceptor materials. However, the random distribution of donor and acceptor materials in such structures can lead to charge trapping at bottlenecks and cul-de-sacs in the conducting pathways to the electrodes. Here, we present a method for growing crystalline organic films into a controlled bulk heterojunction; that is, the positions and orientations of donor and acceptor materials are determined during growth by organic vapour-phase deposition (OVPD[5]), eliminating contorted and resistive conducting pathways while maximizing the interface area. This results in a substantial increase in power conversion efficiency compared with the best values obtained by 'random' small-molecular-weight BHJ solar cells formed by high-temperature annealing, or planar double heterojunction photovoltaic cells using the same archetypal materials systems.

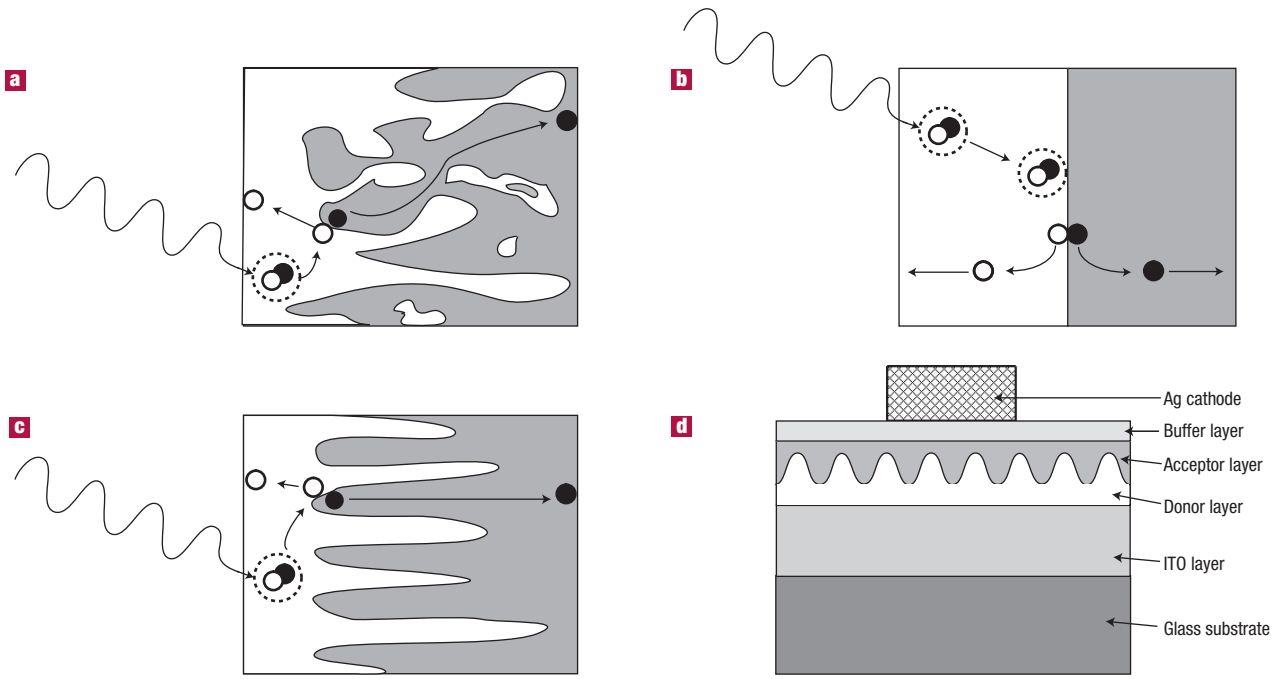

Figure 1 Schematic diagram of the types of organic donor–acceptor heterojunctions and the structure of the controlled bulk heterojunction (BHJ) device. **a**, Thermodynamically driven BHJ formed by phase segregation. The carrier-conducting pathways contain bottlenecks and cul-de-sacs. **b**, Planar heterojunction. **c**, BHJ with a large donor–acceptor interface area and continuous carrier-conducting pathways to the opposing electrodes formed by controlled growth. **d**, Schematic diagram of a controlled BHJ photovoltaic device structure grown on top of indium tin oxide (ITO)-coated glass. The donor material is CuPc and the acceptor is PTCBI. The buffer layer is BCP. Electrons are indicated by closed circles, holes by open circles, and excitons by pairs enclosed in dashed circles.

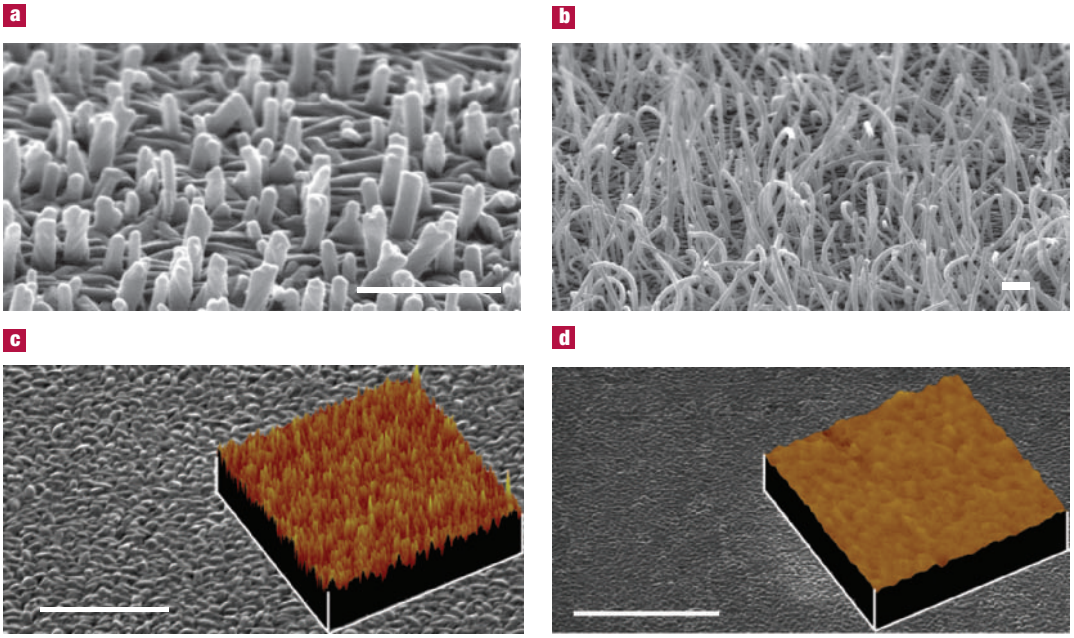

Figure 2 SEM and atomic force microscope (AFM) images of CuPc films. a, Surface of a CuPc film with a continuous wetting layer plus short needle-like crystals grown on a silicon wafer surface by organic vapour phase deposition (OVPD). During a 10-min growth duration, the source evaporation temperature and substrate temperature are fixed at (440 ± 5) °C and (100 ± 5) °C, respectively. The nitrogen carrier gas flow rate is (30.0 ± 0.1) s.c.c.m., and the chamber pressure is (0.45 ± 0.01) torr. **b**, Surface of a CuPc film grown on ITO-coated glass substrate under the same growth conditions as the film in **a**. **c**, Surface of CuPc film grown on top of ITO-coated glass by OVPD. This structure containing a very high density of the protrusions is suitable as the bottom layer of a bulk heterojunction. The source evaporation and substrate temperatures are fixed at (425 ± 5) °C and (100 ± 5) °C, respectively. The nitrogen carrier-gas flow rate increases linearly from 14 s.c.c.m. to 200 s.c.c.m. during the 6.5-min growth duration, and chamber pressure rises from 0.18 torr to 0.70 torr. Inset: AFM image of the same sample. The average peak-to-valley height is 35 nm. **d**, Surface of a 500-Å-thick CuPc film deposited on ITO glass by VTE. Inset: AFM image of the sample with an average peak-to-valley height of 3 nm. Scale bars: all 500 nm.

Bulk heterojunction devices are characterized by an interpenetrating network of donor and acceptor materials, providing a large interface area where photoinduced charge transfer by excitons into separated electrons and holes can efficiently occur (Fig. 1a). In this case, excitons are always generated within a diffusion length (~3–10 nm) of a donor–acceptor interface, potentially leading to a higher cell efficiency than a planar heterojunction (Fig. 1b). Two methods have been reported to make BHJs in organic photovoltaic cells: phase separation during spin-coating of polymers[2,3], and phase segregation from a donor–acceptor mixture induced by high-temperature annealing of small-molecular-weight organic layers[4]. Both of these 'thermodynamically driven' methods have resulted in increased power conversion efficiencies (η_P). For example, in photovoltaic cells based on copper phthalocyanine (CuPc) as the donor and 3,4,9,10-perylenetetracarboxylic bis-benzimidazole (PTCBI) as the acceptor, η_P increases from 1% in a planar heterojunction[1] to 1.4% in devices with a BHJ formed by annealing-induced phase segregation of a homogeneous mixture phase of the two materials[4]. Because of space charge effects in the confines of the BHJ structure, the fill factor (FF) is usually lower than for a planar heterojunction under standard 1-sun illumination (100 mW cm^{-2}) conditions[2,4]. Hence, although the high surface-area characteristic of the BHJ is desirable, the disordered structure is ultimately limited by a high series resistance. In this work, we show that OVPD can be used in the controlled growth of an ordered BHJ (Fig. 1c), largely free of the conductive bottlenecks and cul-de-sacs that are characteristic of thermodynamically driven systems where the interdigitation between the donor and acceptor layers is randomly structured owing to the entropy of the interface formation process.

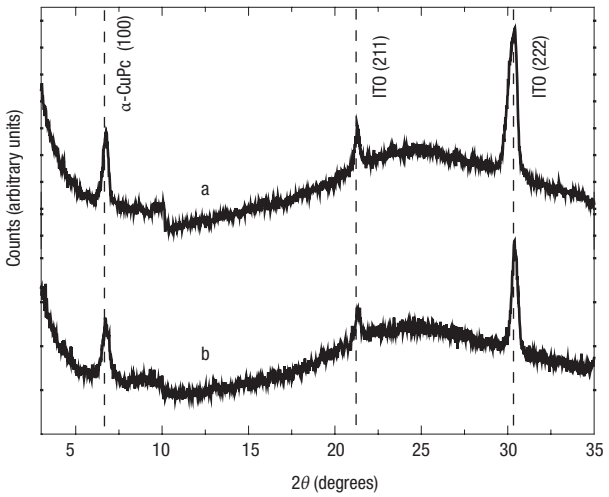

Figure 3 Bragg–Brentano X-ray diffractograms of CuPc films grown on ITO using the Cu-Kα line. a, Diffraction from a CuPc film with a highly folded surface as shown in Fig. 2c. The average film thickness is ~450 Å. **b**, Diffraction from a 500-Å-thick, planar CuPc film grown by VTE, as shown in Fig. 2d. CuPc and ITO crystal indices are noted.

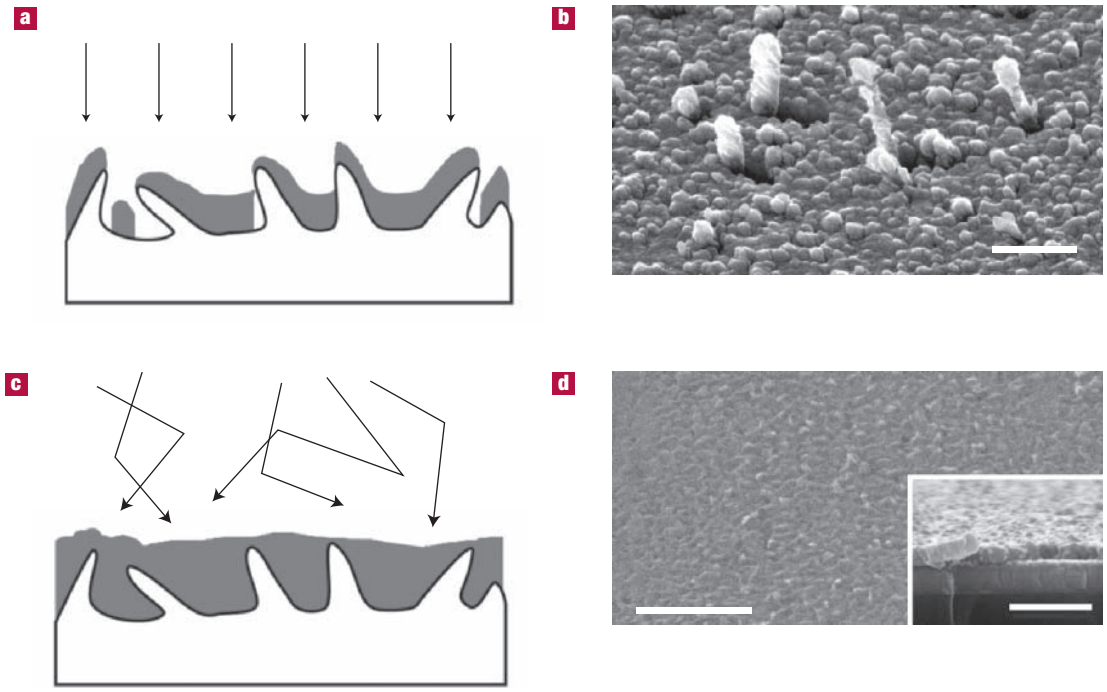

Figure 4 Morphology of films grown on top of a highly folded underlying CuPc layer by VTE and OVPD. a, Schematic diagram of the conformal surface and shadowing effects resulting from the ballistic trajectories followed by the incident molecules in VTE. **b**, SEM image of the surface of a PTCBI/BCP/Ag film grown by VTE on top of CuPc needle arrays. Voids form at the bases of the protruding needles because of shadowing. Note the striations clearly apparent on the sides of the needles, suggesting their crystalline nature. **c**, Schematic diagram of the planar surface and gap-filling characteristic of the top film grown by OVPD that results from increased surface diffusion and random arrival directions of molecules. **d**, SEM images of the planarized surface of a PTCBI layer (500 ± 25) Å thick grown on top of CuPc needles, shown in Fig. 2c. Inset: cross-section of the completed photovoltaic device. From bottom to top, the layers are: glass, ITO (thickness: ~1,500 Å); CuPc/PTCBI/BCP (100 Å); Ag (1,000 Å). Scale bars: all 500 nm.

A schematic of the controlled bulk heterojunction photovoltaic cell is shown in Fig. 1d. The cell is grown on a pre-cleaned, glass substrate coated with 15 Ω/sq. indium tin oxide (ITO), followed by the donor (CuPc) and acceptor (PTCBI) layers, an exciton blocking and electron-conducting layer of bathocuproine (BCP), and finally an Ag cathode. The use of the exciton blocking layer forms a second heterojunction that significantly increases efficiency in thin photovoltaic cells[6]. To form the BHJ, the top surface of the donor layer needs to be highly folded, whereas the acceptor layer should fill the gaps and recesses of the underlying, rough donor film. In addition, the top surface of the acceptor layer should be flat to prevent the formation of shorts or pinholes between the opposing electrodes.

Organic thin-film crystal size and morphology is controllable in OVPD by adjusting the substrate temperature, carrier-gas flow rate and chamber pressure[5,7]. Hence, this technique can prove useful when applied to the growth of both the planar and highly folded layers, as required in a BHJ solar cell. Furthermore, as will be discussed below, a unique and critical feature of OVPD compared with vacuum thermal evaporation (VTE) is the large molecular surface diffusivity and the non-ballistic trajectories followed by the molecules in their arrival at the substrate surface[8]. Hence, OVPD growth is particularly effective in generating planar layers that fill preexisting voids and other surface non-uniformities on the substrate.

In our devices, CuPc and PTCBI are deposited in a quartz reactor that is similar to the glass reactor previously described for the growth of organic thin-film transistors and light emitting devices[7,9]. In contrast to those earlier device demonstrations, however, materials used in photovoltaic cells have considerably higher evaporation temperatures (~450 °C versus ~250 °C for pentacene transistors, for example), requiring modification of the deposition system to prevent material re-evaporation after physisorption on the substrate. With the source evaporation temperature at (440 ± 5) °C, a substrate temperature at (100 ± 5) °C, a nitrogen carrier-gas flow rate of (30.0 ± 0.1) standard cubic centimetres per minute (sccm), and a chamber pressure of (0.45 ± 0.01) torr, a 10-min OVPD strained-layer deposition of CuPc onto a silicon substrate results in a Stranski-Krastonov island-plus-layer growth mode[10], generating the combination of a thin but continuous wetting layer plus short needles, as shown by the scanning electron microscope (SEM) image in Fig. 2a.

Under the same growth conditions, crystalline CuPc needles as long as a few micrometres are grown on ITO-coated glass (Fig. 2b), apparently because of the larger strain between the film and the ITO crystallites, in contrast to the relatively low strain introduced by the thin amorphous oxide layer on the silicon wafer surface. In this case, however, the needle length is ~100 times that required in an efficient photovoltaic cell (about 50 nm).

For high-efficiency charge transfer, the donor–acceptor interface should lie within a diffusion length (~10–50 nm for CuPc) of the exciton generation site. Because a colder substrate favours a higher nucleation density, the substrate temperature is reduced to (16 ± 2) °C, whereas the source material temperature is (425 ± 5) °C. Furthermore, the N_2 flow rate is increased linearly from 14 sccm to 200 sccm during the 6.5-min growth duration, resulting in a rise in chamber pressure from 0.18 to 0.70 torr. In this case, the densely distributed short needles have an average diameter of 30 nm and

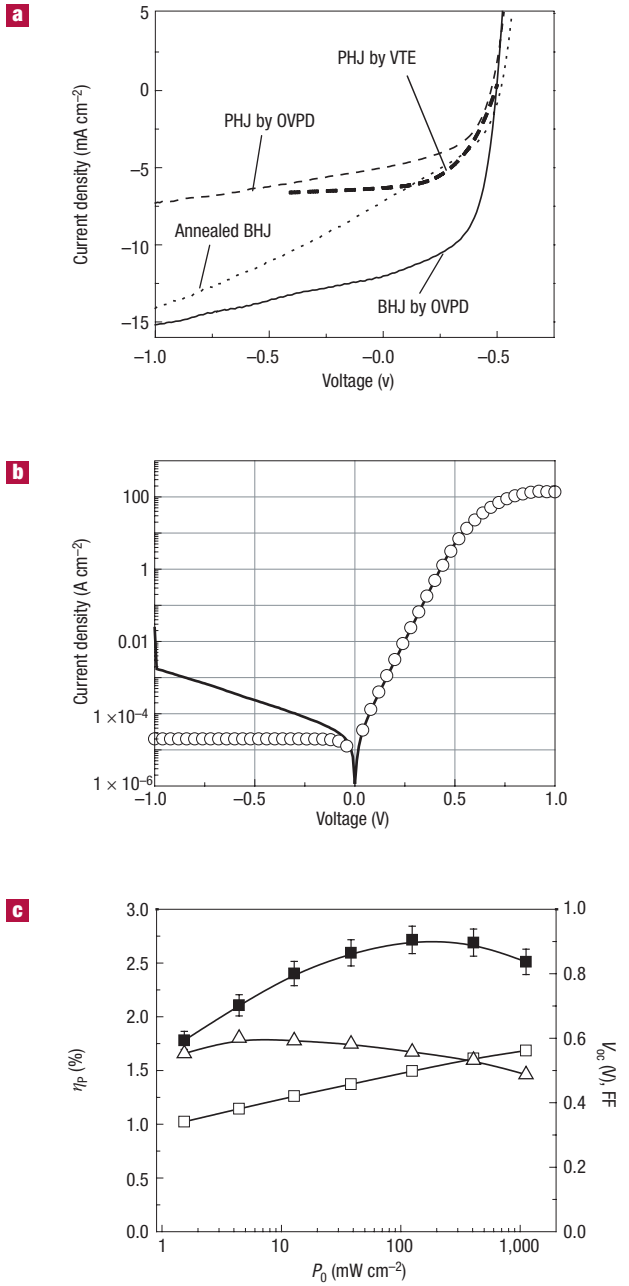

Figure 5 Performance of an OVPD-grown, controlled CuPc/ PTCBI BHJ photovoltaic cell. a, Typical current–voltage characteristics of the BHJ device in comparison with a planar heterojunction (PHJ) produced by OVPD, PHJ by VTE, and BHJ by annealing[4] at incident power level of 1 sun using AM1.5G simulated solar irradiation. The open-circuit voltages are similar for all CuPc/PTCBI cells, and the maximum photocurrent density is achieved in the BHJ device by OVPD. The comparison of device characteristics is listed in Table 1. **b**, Fit of the dark *J–V* characteristics of the OVPD BHJ device, where the solid line is the experimental data, and the circles are a fit according to the modified ideal diode equation. Under reverse bias, the dark current is higher than predicted by this simple analysis owing to the presence of current sources other than diffusion (for example, generation–recombination and shunt currents may also be present). **c**, The power conversion efficiency, η_P (closed squares), open-circuit voltage, V_{OC} (open squares), and fill factor, FF (triangles), as functions of the incident optical power intensity P_0 for the OVPD-grown, controlled CuPc/PTCBI BHJ photovoltaic device. A maximum power efficiency at 1 sun (100 mW cm^{-2}) intensity of $\eta_P = (2.7 \pm 0.1)\%$ is obtained, a value significantly higher than is achieved for planar or 'random' BHJ structures previously reported for this archetypal materials system for photovoltaic cells.

peak-to-valley height of 35 nm, corresponding to 70% of the mean thickness of the CuPc film (Fig. 2c). In contrast, the average peak-to-valley height of a vacuum-deposited CuPc film of the same thickness is only 3 nm (Fig. 2d).

The X-ray diffraction spectrum of the OVPD CuPc film is shown in Fig. 3a, and is similar to that of a 500-Å-thick CuPc film grown by vacuum thermal evaporation (Fig. 3b). The diffraction peak at $2\theta = 6.7°$ confirms the existence of the α-CuPc phase. The domain size is calculated to be (20 ± 5) nm from the full width at half maximum of the diffraction peak[11], from which we infer that each small protrusion in Fig. 2c is a single CuPc microcrystalline domain. Because the charge mobility is higher in crystalline than in amorphous materials[12,13], the existence of crystalline structures is important for ensuring a low cell series resistance.

Growth of CuPc is followed by that of a PTCBI layer (500 ± 25) Å thick without exposing the interface to atmosphere. To ensure a flat surface, the source material is heated to (462 ± 3) °C, while the substrate is maintained at (16 ± 5) °C. The N_2 flow rate is fixed at (150 ± 1) sccm for 10.4 min, resulting in a chamber pressure of (0.58 ± 0.01) torr. A 100-Å-thick BCP exciton-blocking and electron-conducting layer and a 1,000-Å-thick silver circular cathode contact (1 mm^2) deposited through a shadow mask are grown by conventional vacuum thermal evaporation to complete the photovoltaic cell.

In VTE, the deposited film typically has a morphology that conforms to the underlying surface, resulting in some shadowed areas (see Fig. 4a), owing to the long mean free paths and ballistic trajectories followed by the incident molecules. Hence, the PTCBI surface follows that of the CuPc protrusions, also resulting in a second, highly folded top surface. In that case, voids will develop where the protrusions shadow the underlying surface of the film from the PTCBI source cell (Fig. 4b). Although these problems can be reduced (but not eliminated) by using substrate rotation, this can increase the processing cost and also prohibit adaptation for continuous roll processing, which is more easily accomplished by the conformal character of OVPD. The diagonal striations on the edges of the needles give a further suggestion of their crystalline nature. In contrast, in OVPD growth, surface diffusion coupled to the random arrival directions as the molecules traverse the boundary layer at the substrate surface[8] results in a flattened top film surface with complete filling of the spaces beneath the needles in the underlying CuPc, as shown in Fig. 4c and d.

For comparison to the bulk heterojunction photovoltaic cell, we also grew a planar heterojunction ITO/450 Å CuPc/500 Å PTCBI/100 Å BCP/1,000 Å Ag. The planar CuPc layer was deposited for 3 min with a source temperature of (445 ± 3) °C, a substrate temperature of (3 ± 5) °C, and a N_2 flow rate of (100 ± 1) sccm. The PTCBI is deposited under the same conditions as used for the BHJ device.

The current density–voltage characteristics of the BHJ and other double heterojunction CuPc/PTCBI photovoltaic cells are combined in Fig. 5a, whose performances are compared in Table 1. The short-circuit current density (J_{SC}) for the controlled BHJ is about twice that obtained for a vacuum-deposited[6] or OVPD-grown planar heterojunction photovoltaic cell. Furthermore it is about 20% higher than for a previously reported 'thermodynamically driven' BHJ demonstrated by annealing a mixed CuPc/PTCBI layer[4]. More significantly, the dependence of the photocurrent on reverse bias of the grown BHJ is considerably reduced from that observed for the annealed device. We fitted the dark-current density characteristics using the ideal diode equation including series resistance that has been previously shown to apply to molecular organic photovoltaic devices[6,14,15]. From Fig. 5b, showing the fit (circles) to the data (solid line), we infer a specific series resistance of $R_{SA} = (2.2 \pm 0.1)\ \Omega\ \text{cm}^2$, which is smaller than the value obtained from a random BHJ device[4]

Table 1 Comparison of performance of several ITO/CuPc/PTCBI/BCP/Ag photovoltaic cell structures*

	J_{sc} (mA cm^{-2})	V_{OC} (V)	FF	η_P (%)	R_{SA} (Ω cm^2)	Ref.
Planar VTE heterojunction	6	0.49	0.49	1.1 ± 0.1	30 ± 10	6
Annealed bulk heterojunction	9	0.50	0.40	1.4 ± 0.1	60 ± 10	4
Planar OVPD heterojunction	5	0.48	0.47	1.1 ± 0.1	18.2 ± 0.5	This work
Controlled bulk OVPD heterojunction	11	0.49	0.58	2.7 ± 0.1	2.2 ± 0.1	This work

Here, J_{sc} is the short-circuit current density, V_{OC} is the open-circuit voltage, FF is the fill factor, η_P is the external power efficiency and R_{SA} is the specific series resistance.

*The illumination intensity is 1 sun (100 mW cm^{-2}) simulated AM1.5G for all four devices.

where $R_{SA} = (60 \pm 10)\ \Omega\ cm^2$. This suggests that series resistance due to the amorphous growth, or to bottlenecks to carrier collection has been reduced in the OVPD-grown BHJ cell.

The dependence of the performance characteristics under illumination is shown in Fig. 5c. For control, we obtain a 1% power-conversion efficiency for a conventional CuPc/PTCBI bilayer cell[1] under AM1.5G illumination using a calibrated solar simulator[6], which is consistent with efficiencies reported elsewhere[16,17]. In the case of the BHJ cell, using 1-sun-intensity, AM1.5G simulated radiation, we obtain an open-circuit voltage of $V_{OC} = (0.50 \pm 0.03)$ V at 1 sun intensity (100 mW cm^{-2}), characteristic of the CuPc/PTCBI heterojunction system. The fill factor of the OVPD-grown, controlled BHJ device is FF > 0.5 for illumination over the range of 0.01–10 suns (1–1000 mW cm^{-2}). The combination of high photocurrent density and fill factor results in a high external power conversion efficiency (η_P), with a maximum of $\eta_P = (2.7 \pm 0.1)\%$ at 100 mW cm^{-2}. Referring to Table 1, η_P is about 2.5 times as high as was achieved using a comparable planar heterojunction photovoltaic cell, and 1.9 times as high as an annealed, thermodynamically driven BHJ, suggesting that the controlled growth of the CuPc/PTCBI BHJ results in the desired increase in junction surface area without introducing an increased cell series resistance. Because the CuPc crystal sizes deduced from X-ray diffraction are the same (~20 nm) for the OVPD-grown BHJ and the previously reported annealed BHJ[4], we infer that the increase in efficiency is mainly due to the larger carrier-transport efficiency in a highly ordered bulk heterointerface. In addition, we have observed that the power efficiency of an OVPD-grown CuPc/C_{60} BHJ device is the same as a VTE-grown CuPc/C_{60} mixed layer heterojunction[18], from which we can also infer that the large interface area plays a significant role.

This work opens several new avenues for controlling the thin-film morphology of organic heterojunction devices, and has already resulted in a striking increase in efficiency for an organic BHJ solar cell. We expect that further understanding and control of the unique growth properties characteristic of OVPD will produce further improvements in the performance of organic photovoltaic and other optoelectronic devices.

Received 16 July 2004; accepted 18 October 2004; published 12 December 2004.

References

1. Tang, C. W. Two-layer organic photovoltaic cell. *Appl. Phys. Lett.* **48,** 183–185 (1986).
2. Yu, G., Gao, J., Hummelen, J. C., Wudl, F. & Heeger, A. J. Polymer photovoltaic cells: enhanced efficiencies via a network of internal donor-acceptor heterojunctions. *Science* **270,** 1789–1791 (1995).
3. Halls, J. J. M. *et al.* Efficient photodiodes from interpenetrating polymer networks. *Nature* **376,** 498–500 (1995).
4. Peumans, P., Uchida, S. & Forrest, S. R. Efficient bulk heterojunction photovoltaic cells using small-molecular-weight organic thin films. *Nature* **425,** 158–162 (2003).
5. Baldo, M. *et al.* Organic vapor phase deposition. *Adv. Mater.* **10,** 1505–1514 (1998).
6. Peumans, P., Bulovi , V. & Forrest, S. R. Efficient photon harvesting at high optical intensities in ultrathin organic double-heterostructure photovoltaic diodes. *Appl. Phys. Lett.* **76,** 2650–2652 (2000).
7. Shtein, M., Mapel, J., Benziger, J. B. & Forrest, S. R. Effects of film morphology and gate dielectric surface preparation on the electrical characteristics of organic-vapor-phase-deposited pentacene thin-film transistors. *Appl. Phys. Lett.* **81,** 268–270 (2002).
8. Shtein, M., Peumans, P., Benziger, J. B. & Forrest, S. R. Micropatterning of small molecular weight organic semiconductor thin films using organic vapor phase deposition. *J. Appl. Phys.* **93,** 4005–4016 (2003).
9. Shtein, M., Gossenberger, H. F., Benziger, J. B. & Forrest, S. R. Material transport regimes and mechanisms for growth of molecular organic thin films using low-pressure organic vapor phase deposition. *J. Appl. Phys.* **89,** 1470–1476 (2001).
10. Venables, J. A., Spiller, G. D. T. & Hanbücken, M. Nucleation and growth of thin films. *Rep. Prog. Phys.* **47,** 399–459 (1984).
11. Klug, H. P. & Alexander, L. E. *X-ray Diffraction Procedures* (Wiley, New York, 1974).
12. Forrest, S. R. Ultrathin organic films grown by organic molecular beam deposition and related techniques. *Chem. Rev.* **97,** 1793–1896 (1997).
13. Makinen, A. J., Melnyk, A. R., Schoemann, S., Headrick, R. L. & Gao, Y. Effect of crystalline domain size on the photophysical properties of thin organic molecular films. *Phys. Rev. B* **60,** 14683–14687 (1999).
14. Xue, J., Uchida, S., Rand, B. P. & Forrest, S. 4.2% efficient organic photovoltaic cells with low series resistances. *Appl. Phys. Lett.* **84,** 3013–3015 (2004).
15. Hoppe, H. & Sariciftci, N. S. Organic solar cells: an overview. *J. Mater. Res.* **19,** 1924–1945 (2004).
16. Rostalski, J. & Meissner, D. Photocurrent spectroscopy for the investigation of charge carrier generation and transport mechanisms in organic p/n-junction solar cells. *Solar Energy Mater. Solar Cells* **63,** 37–47 (2000).
17. Sharma, G. D. & Saxena, D. Characterization of ITO/ZnPc/CHR/In p-n junction photovoltaic device using *J-V*, *C-V* and photoaction measurements. *J. Mater. Sci.* **10,** 539–544 (1999).
18. Uchida, S., Xue, J., Rand, B. P. & Forrest, S. Organic small molecule solar cells with a homogeneously mixed copper phthalocyanine: C_{60} active layer. *Appl. Phys. Lett.* **84,** 4218–4220 (2004).

Acknowledgements

We thank J. Xue, S. Uchida, R. Holmes, B. Rand and P. Peumans for discussions. We also thank the US Air Force Office of Scientific Research, the National Renewable Energy Laboratory and Global Photonic Energy Corporation for financial support.

Correspondence and requests for materials should be addressed to S.R.F.

Competing financial interests

The authors declare that they have no competing financial interests.